Int J Fract (2025) 249:43
https://doi.org/10.1007/s10704-025-00856-0

RESEARCH

# Identifying simple shear in plane stress states

**Lilia Schuster · Sebastian Münstermann**

Received: 6 September 2024 / Accepted: 15 May 2025


**Abstract** Modern phenomenological damage models use Lode parameter $L$ and triaxiality $\eta$ to describe the stress state of an isotropic material. Value pairs in the region between $L, \eta = (0, 0)$ and $L, \eta = (0, \frac{1}{\sqrt{3}})$ in plane stress condition can lead to ambiguous descriptions of the deformation. The case of simple shear is not defined separately. By using the difference in angles between the principal strain and principal stress axes, cases of coaxial stretch superposed with simple shear can be distinguished from cases of coaxial stretch without simple shear. In the case of anisotropic material or large elements, the distinction between these ambiguous cases can be utilized to optimize failure models. This study proposes a method to recover the deformation gradient and shear direction for proportional and non-proportional loading with an elastoplastic von Mises material. The deformation gradient is suitable for distinguishing stress states with simple shear from stress states without simple shear in plane stress condition.

**Keywords** Simple shear · Lode parameter · Triaxiality · Fracture locus · Damage mechanics · Non-coaxial deformation

## 1 Introduction

Established phenomenological damage models rely on the use of triaxiality $\eta$ and Lode parameter $L$ to describe the stress state Bai and Wierzbicki (2008); Mohr and Marcadet (2015); Lian et al. (2013); Lou et al. (2012); Brünig et al. (2016); Liu et al. (2022); Ganjiani and Homayounfard (2021); Cao et al. (2014). The calculation of these values is commonly based on the principal stresses $\sigma_1$, $\sigma_2$ and $\sigma_3$, with triaxiality $\eta$ calculated as the ratio between the mean stress and von Mises stress, that is $\eta = \frac{\sigma_1+\sigma_2+\sigma_3}{3\sqrt{0.5((\sigma_1-\sigma_2)^2+(\sigma_2-\sigma_3)^2+(\sigma_3-\sigma_1)^2)}}$ and Lode parameter $L$ calculated with $L = \frac{2\sigma_2-\sigma_1-\sigma_3}{\sigma_1-\sigma_3}$. The calibration of phenomenological damage models is a challenging task because it requires extensive testing programs to cover a wide range of stress states. The resulting fracture locus is often highly dependent on the selection of calibration tests. A proportional loading path that ensures constant values of triaxiality and Lode parameter is important to perform a reliable calibration of the damage model. Therefore, many studies deal with the design of test setups and specimen geometries

**Supplementary Information** The online version contains supplementary material available at https://doi.org/10.1007/s10704-025-00856-0.

L. Schuster (✉)
wbk Institute of Production Science, Manufacturing and Materials Technology, Karlsruhe Institute of Technology, Kaiserstr. 12, 76131 Karlsruhe, Germany
e-mail: lilia.schuster@kit.edu

S. Münstermann
Institute of Metal Forming, RWTH Aachen University, Intzestr. 10, 52072 Aachen, Germany
e-mail: sebastian.muenstermann@ibf.rwth-aachen.de

Published online: 10 June 2025

to achieve specific stress states Traphöner et al. (2021); Roth and Mohr (2016). For example, proportional loading paths for simple shear can be achieved by using disc specimens under torsional loading Traphöner et al. (2018, 2021); Yin et al. (2015); Grolleau et al. (2022). In some cases, a variety of conditions can be produced with the same specimen geometry by rotating the specimen during loading Anderson et al. (2017) or by applying forces along two different axes Brünig et al. (2016); Barsoum and Faleskog (2007). In addition to selecting the right calibration tests, the specimens must be prepared and manufactured with high accuracy. A deficient surface quality of the testing specimens Traphöner et al. (2018) or edge cracking effects Habibi et al. (2023) can have detrimental effects on the fracture strain and influence the shape of the fracture locus.

Wierzbicki and Xue (2005) proposed the construction of a failure surface that describes the plastic failure strain $\varepsilon_{eq}^{pl}$ as a function of the stress state. The stress state is described by triaxiality and Lode parameter. The principal values of the Cauchy stress tensor are $\sigma_1$, $\sigma_2$ and $\sigma_3$. The principal stress values are used to calculate the mean stress $\sigma_m$ and the von Mises equivalent stress $\sigma_{vM}$. These values serve to calculate the triaxiality $\eta$ as the ratio between mean stress and von Mises stress. Three variations of expressing the Lode parameter are common in literature; the Lode parameter as the distance between origin and deviatoric plane in Haigh-Westergaard stress space $\xi$, the normalized Lode angle $\bar{\theta}$ and the Lode parameter $L$. Additionally, in geology Lode's ratio $\nu$ is used. The Lode parameter was introduced in 1926 to describe deformed metal Lode (1926). But it was more commonly used in structural geology, where it is used to describe the ellipsoidal shape of the 3D representation of strain Elliott (1972). The interpretation of the Lode parameter is to define whether the strain ellipsoid is oblate, prolate, or spherical (Fig. 1). Diagrams, such as the Hsu / Hossack diagram and the Flinn diagram indicate the ratio of stretch in the principal stretch directions in dependence of a strain intensity value $\bar{\varepsilon}$. These diagrams are common tools in geology Hsu (1966); Hossack (1968); Ramsay and Huber (2003).

One commonly overlooked aspect is that a stress state described by Lode parameter $L$ and triaxiality $\eta$ is ambiguous. This ambiguity is particularly noticeable for shear. The stress state typically referred to as shear, is described by Lode parameter $L$ and triaxiality $\eta$ both at zero. However, this stress state can result from either

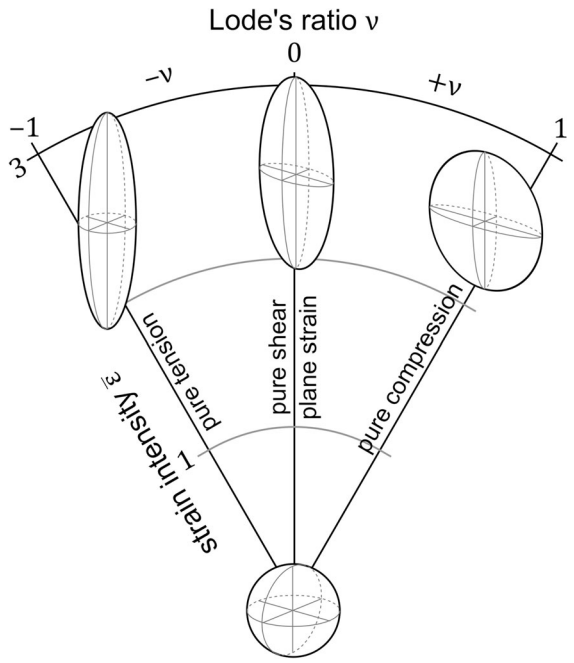


**Fig. 1** The Hsu diagram describes the shape of the strain ellipsoid via Lode's ratio $\nu = (2\varepsilon_2 - \varepsilon_1 - \varepsilon_3)/(\varepsilon_1 - \varepsilon_3)$

pure shear or simple shear Butcher and Abedini (2019). Pure shear results, when a square stretches in one direction, so that all angles remain at right angles and the edge in direction of zero stress keeps its length. Simple shear results when two sides of a square slide in opposite directions, so that all opposite edges remain parallel to one another. This stress state is what we typically think of when we talk about shear.

However, any value pair of Lode parameter and triaxiality in the range of $L, \eta = (0, 0)$ and $L, \eta = (0, \frac{1}{\sqrt{3}})$ in plane stress condition can result from a superposed deformation of stretch and simple shear. In (Fig. 2) the triaxiality $\eta$ and Lode parameter $L$ are evaluated using the equations explained above. The strain paths describing the stress state during the deformation of the two cubic elements coincide. It seems unintuitive that the stress state described by $L, \eta = (-1, \frac{1}{3})$, which is known as a uniaxial stress state, can have a simple shear component. This issue is typically not addressed. All stress states described by the same value pair of Lode parameter and triaxiality are assumed to describe the same stress state, regardless of whether simple shear is present. Two animated versions of the deformations corresponding to uniaxial tension shown in Fig. 2 can be found in Electronic Supplementary Material 1 (for

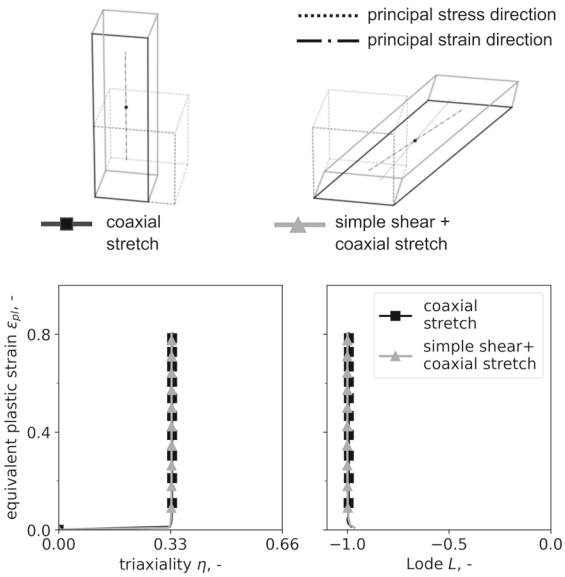


**Fig. 2** Different deformations of initially cubic elements following identical proportional strain paths at $L, \eta = (-1, \frac{1}{3})$ under plane stress with a von Mises material

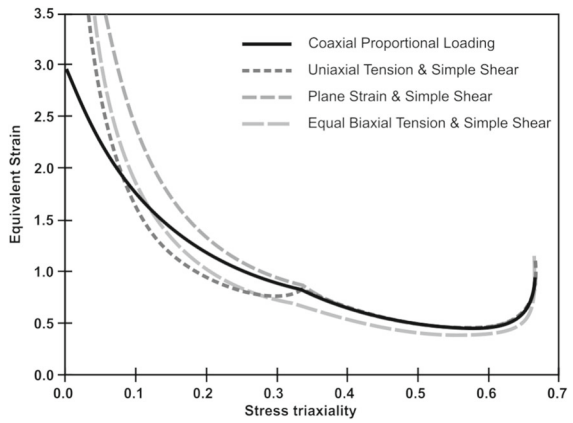


**Fig. 3** Failure loci obtained from traversing different paths of an isotropic material under plane stress loading conditions (adapted from Butcher and Abedini (2019) Fig. 15, used under CC BY 4.0)

2D view) and Electronic Supplementary Material 2 (for 3D view).

Current descriptions of stress states using Lode parameter and triaxiality are not suitable for finding the presence and magnitude of simple shear. When transforming deformation gradients to strain tensors the information regarding simple shear is lost. Therefore, this problem persists when Lode parameter and triaxiality are calculated in strain space Lou et al. (2014). It is treated the same way as a body undergoing pure shear and rigid body rotation Ramsay and Huber (2003). To identify the presence of a simple shear component it is necessary to calculate the angular difference between the principal stress and principal strain axes. The principal stress and principal strain axes will always remain coaxial without simple shear, but they will diverge as simple shear progresses Ramsay and Huber (2003).

Unit cell calculations performed by Vigneshwaran and Benzerga (2023) show that the magnitude of the shear component for a shear-tension loading affects the onset of localization and ductility. The need to distinguish simple shear and pure shear is in accordance with geology studies Ramsay and Huber (2003). During simple shear, some directions in the material undergo sequences of shortening and stretching. Whereas in pure shear, all directions progressively either lengthen or shorten Ramsay and Huber (2003).

In Butcher and Abedini (2019) the authors concluded that Lode angle and stress triaxiality are insufficient to uniquely describe a stress state. Their study revealed that the fracture locus for plane stress cannot be described by a 2D failure curve as previously assumed. Even for plane stress, the fracture locus must be described by three dimensions. From their study in Butcher and Abedini (2019) it is evident that the discontinuity at uniaxial stress of the plane stress failure curve, as commonly described in literature Bai and Wierzbicki (2008), is an artifact of mixing coaxial and non-coaxial calibration tests. Specifically, when characterization tests of simple shear (non-coaxial) for $L, \eta = (0, 0)$ and uniaxial loading (coaxial) $L, \eta = (-1, \frac{1}{3})$ are utilized to calibrate the failure curve, a discontinuity and local maximum at uniaxial tension results. If only calibration tests with no simple shear component were utilized to calibrate the failure curve, the value of equivalent strain at triaxility $\eta = 0$ would be higher and the failure curve would transition to values $\eta > \frac{1}{3}$ without the formation of a peak. They concluded that distinguishing between simple shear and pure shear is necessary when developing failure models and proposed a failure surface for plane stress based on triaxiality and a newly introduced normalized shear angle parameter, which takes the coaxilaity into consideration. However, to calculate this normalized shear angle parameter the shear deformation needs to be oriented parallel to one of the local coordinate axes and loading needs to remain proportional. These conditions can rarely be expected in practical applications.

The present paper will show a method to retrieve information regarding simple shear for isotropic incompressible materials under plane stress for deformations resulting from superposed simple shear and coaxial stretch for proportional and non-proportional loading. This presented method is robust to rigid body rotation and translation. Boundary conditions are presented to create one-element tests for specific stress states with and without simple shear for plane stress in regions of low triaxialities.

## 2 Materials and Methods

In this section, we will look at established equations and parameters to describe the stress state of a material. The equations and parameters will be discussed in the context of simple shear.

### 2.1 Stress states defined by Lode parameter and triaxiality

Phenomenological failure models use different variables derived from the stress invariants to describe the stress state of a material. Failure models developed by Johnson-Cook Johnson and Cook (1985) or Hancock-Mackenzie Hancock and Mackenzie (1976) describe a fracture strain dependent on triaxiality. Triaxiality depends on the first invariant of the stress tensor $I_1$ and the second invariant of the deviatoric stress tensor $J_2$. These descriptions of the fracture locus were extended by Bai and Wierzbicki to include the dependence on the Lode parameter Wierzbicki and Xue (2005). The Lode parameter is a measure derived from the third invariant of the stress tensor $J_3$.

$$p = -\frac{1}{3}I_1 = -\sigma_m = -\frac{1}{3}(\sigma_1 + \sigma_2 + \sigma_3) \tag{1}$$

$$q = \sqrt{3J_2} = \sigma_{vMises} = \sqrt{\frac{1}{2}\left[(\sigma_1 - \sigma_2)^2 + (\sigma_2 - \sigma_3)^2 + (\sigma_3 - \sigma_1)^2\right]} \tag{2}$$

$$r = \left[\frac{27}{2}(\sigma_1 - \sigma_m)\cdot(\sigma_2 - \sigma_m)\cdot(\sigma_3 - \sigma_m)\right]^{\frac{1}{3}} \tag{3}$$

$$\eta = -\frac{p}{q} \tag{4}$$

$$\xi = \frac{J_3}{2}\left(\frac{3}{J_2}\right)^{\frac{3}{2}} = \left(\frac{r}{q}\right)^3 = \cos(3\theta) \tag{5}$$

$$\overline{\theta} = 1 - \frac{6\theta}{\pi} = \frac{2}{\pi}\arccos\xi \tag{6}$$

$$L_\sigma = \frac{3\cdot\tan(\theta) - \sqrt{3}}{\tan(\theta) + \sqrt{3}} \tag{7}$$

In material science, the Lode parameter is commonly defined in terms of stress values as seen in Eqs. 5 to 7. The definition of Lode parameter and triaxiality depending on strain values was introduced to materials science by Lou et al. Lou et al. (2014). The equation to calculate the Lode parameter is based on true strain increments (Eq. 8).

$$L_\varepsilon = \frac{3d\varepsilon_2}{d\varepsilon_1 - d\varepsilon_3} \tag{8}$$

The values $d\varepsilon_1, d\varepsilon_2, d\varepsilon_3$ are the increments of principal true strain. Their indices describe the order of their magnitudes with $\varepsilon_1 \geq \varepsilon_2 \geq \varepsilon_3$. These values do not contain information about the direction or orientation of the principal strain axis. Under the assumption of proportional loading, the triaxiality $\eta_\varepsilon$ can then be calculated with Eq. (9), which was derived in Lou et al. (2014). The exact definition of $\eta_\varepsilon$ depends on which principal stress equals zero.

$$\eta_\varepsilon(L_\varepsilon) = \begin{cases} -\frac{3-L_\varepsilon}{3\cdot\sqrt{{L_\varepsilon}^2+3}}, & \sigma_1 = 0 \\ -\frac{2\cdot L_\varepsilon}{3\cdot\sqrt{{L_\varepsilon}^2+3}}, & \sigma_2 = 0 \\ \frac{3+L_\varepsilon}{3\cdot\sqrt{{L_\varepsilon}^2+3}}, & \sigma_3 = 0 \end{cases} \tag{9}$$

However, Lode parameter and triaxiality can not be arbitrarily transformed from stress space to strain space and vice versa when the underlying deformation gradient superposes simple shear and coaxial stretch. Therefore, we will be using the subscript $\varepsilon$ throughout this study, to indicate $L_\varepsilon$ calculated by Eq. (8) and $L_\sigma$ calculated by 7. These two equations can give two different results and are not always interchangeable.

### 2.2 Stress states defined in a spherical coordinate system

In Butcher and Abedini (2019), the authors identified the ambiguous nature of $L_\sigma$, $\eta_\sigma$ descriptions for stress states and aimed to create a framework that allows to differentiate the shear and normal part by using a spherical coordinate system (4). The framework is limited to plane stress states and assumes $\sigma_3$ to be zero. The spherical coordinates were calculated with Eq. (10) and Eq. (11). The radius is the von Mises stress in plane

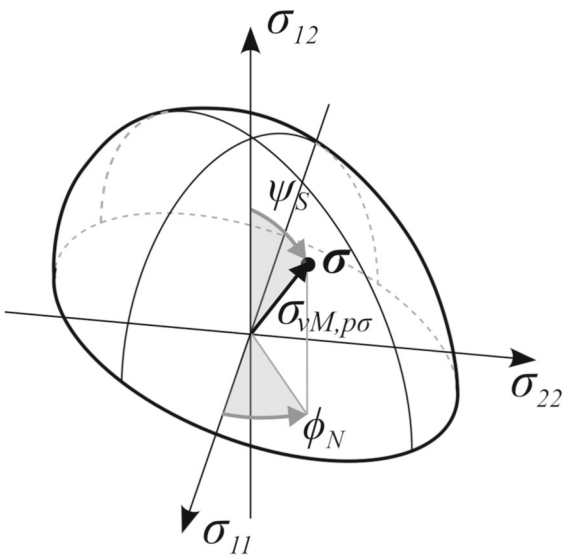


**Fig. 4** Spherical coordinate system for stress states in plane stress according to Butcher and Abedini (2019)

stress. The shear angle $\psi_S$ and normal angle $\phi_N$ can assume values between 0° and 90°.

$$\begin{aligned}\sigma_{12} &= \sigma_{vM,p\sigma} \cdot \cos\ \psi_S \\ \sigma_{11} &= \sigma_{vM,p\sigma} \cdot \cos\ \phi_N \cdot \cos\ \psi_S \\ \sigma_{22} &= \sigma_{vM,p\sigma} \cdot \sin\ \phi_N \cdot \sin\ \psi_S \end{aligned} \tag{10}$$

$$\sigma_{vM,p\sigma} = \sqrt{0.5 \cdot \left((\sigma_{11} - \sigma_{22})^2 + {\sigma_{11}}^2 + {\sigma_{22}}^2 + 6{\sigma_{12}}^2\right)} \tag{11}$$

Any stress tensor can be presented in this coordinate system by a point on the yield surface. Some points on this surface represent special stress states. These stress states are indicated in Fig. 5. Therefore, the equivalent plastic strain depends on the path traversed on the yield surface. Three paths are shown in Fig. 5.

The authors showed that even for plane stress, the fracture locus must be described by three dimensions, where the strain to fracture is dependent on two parameters, i.e. $\psi_S$, $\phi_N$ or $\psi_S$, $\eta_\sigma$. We will show that using $\psi_S$, $\eta_\sigma$ the stress state descriptions are not unique, but a fracture locus defined in $\psi_S$, $\phi_N$ is advantageous compared to the $L_\sigma$, $\eta_\sigma$ fracture locus in plane stress.

## 2.3 Deformation gradient

So far, we have not seen a distinctive treatment of simple shear for cases in which simple shear is superposed

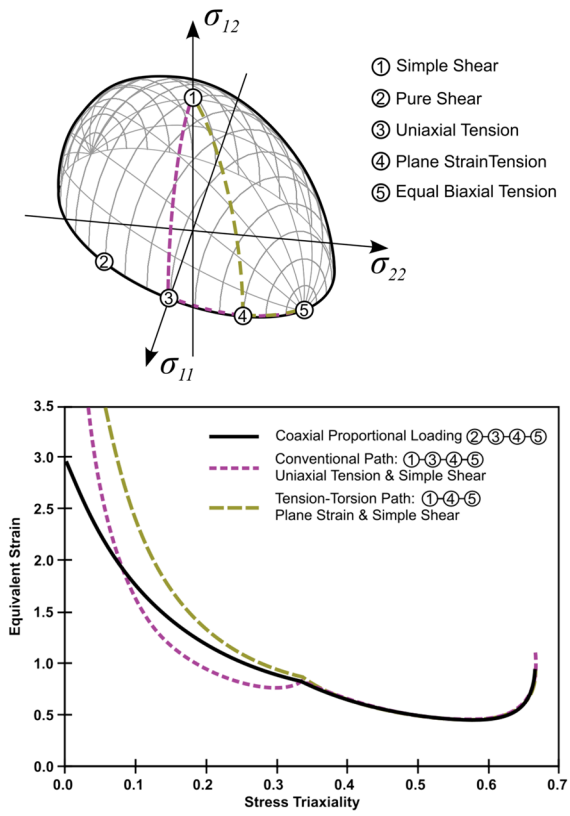


**Fig. 5** Fracture loci generated along paths with coaxial and non-coaxial stress states (adapted from Butcher and Abedini (2019) Fig. 14, used under CC BY 4.0)

with uniaxial stretch. The question is how simple shear is defined, what its physical meaning is, and where in the definitions of stress state, that we have used up to this point, we can find the simple shear component.

We have already defined simple shear as a deformation that moves two opposite edges of an element and transforms it into a parallelogram. The resulting strain is rotational. A rotational strain means that the principal axis of strain will rotate during deformation. In structural geology, the deformation history is described as progressive deformation and deals with various changes of the deformation gradient over time Ramberg (1975); Elliott (1972). Pure shear is a deformation where each side of the deformed cubed remains constant in area size, while the aspect ratio of the sides may differ but remain rectangular. The resulting strain is irrotational. Any 2D deformation that can neither be classified as simple shear nor pure shear is called general shear.

In the components of the deformation gradient, simple shear can easily be spotted when either of the off-diagonal entries is different from zero. To get from the deformation gradient to our familiar terms of describing the stress state with Lode parameter and triaxiality, several transformations are required. These transformations will get us to the principal strain tensor, which we can then use to derive our familiar quantities of the Lode parameter and triaxiality.

First, the deformation gradient containing a superposition of simple shear along the x-axis with uniaxial stretch in the xy - plane is defined (Eq. 12). The stretch is only uniaxial in the xy - plane and a change in length also occurs in z-direction. According to our nomenclature introduced in Fig. 8 this loading case is simple shear with parallel uniaxial stretch.

$$F = \begin{bmatrix} 1+dx & \gamma & 0 \\ 0 & 1 & 0 \\ 0 & 0 & \frac{1}{1+dx} \end{bmatrix} \tag{12}$$

The polar decomposition of the deformation gradient $F$ will decompose the deformation gradient into a rigid body rotation tensor and a stretch tensor (Eq. 13). For a right-hand polar decomposition, the element is first stretched then rotated, i.e. $F = R \cdot U$; for a left-hand polar decomposition, the element is first rotated then stretched, i.e. $F = V \cdot R$. Where $U$ is called the right stretch tensor and $V$ the left stretch tensor.

$$F = R \cdot U = V \cdot R \tag{13}$$

With the eigenvalues of the stretch tensor $\lambda_1, \lambda_2, \lambda_3$ the stretch tensor can be written in terms of engineering strains (Eq. 14).

$$\begin{aligned} U &= \begin{bmatrix} \lambda_1 & 0 & 0 \\ 0 & \lambda_2 & 0 \\ 0 & 0 & \lambda_3 \end{bmatrix} \\ &= \begin{bmatrix} 1+\varepsilon_{1,eng} & 0 & 0 \\ 0 & 1+\varepsilon_{2,eng} & 0 \\ 0 & 0 & 1+\varepsilon_{3,eng} \end{bmatrix} \end{aligned} \tag{14}$$

The engineering strains are readily transformed into true strains with $\varepsilon_{1,true} = \log(\varepsilon_{1,eng} + 1)$, giving us the principal strain tensor (Eq. 15).

$$\varepsilon_{princ} = \begin{bmatrix} \varepsilon_{1,true} & 0 & 0 \\ 0 & \varepsilon_{2,true} & 0 \\ 0 & 0 & \varepsilon_{3,true} \end{bmatrix} \tag{15}$$

As we can see, the principal strain tensor does not contain any information about the original orientation of the element. In fact, at this point, the information of simple shear is only contained in the rigid body rotation tensor R (Eq. 13). The true strain tensor can be rotated back to the original coordinate system with $\varepsilon_{xyz} = R^T \cdot \varepsilon_{princ} \cdot R$. But that would not provide information about the original shear involved. It would simply change the directions we define as x, y, and z. With this approach, we are not able to see whether we are dealing with simple shear or whether the element just rotated in space because of rigid body movement.

To illustrate this, the transformations for three deformation gradients are presented (Fig. 6). Lode parameter and triaxiality were calculated by finite element simulation. We can now see that for all these three cases we arrive at the same pair of Lode angle and triaxiality. The information about simple shear seems to be lost. Our common quantities do not provide any way to recover this information.

We will aim to find a way to distinguish these three cases. We will also look at different deformation gradients superposing simple shear with uniaxial stretch in the plane of non-zero stresses and how to find deformation gradients for each case at any Lode parameter and triaxiality pair.

### 2.4 Mohr's circle for strains

Means Means (1982, 1983) demonstrated how Mohr's circle can be used to represent asymmetric second-order tensors. This representation is especially useful for visualizing the deformation gradient Eq. (16). This version of Mohr's circle is commonly used in geology to describe the final deformation state of a volume of rock Passchier (1988). In the field of geology, the issue that simple shear has to be treated separately from pure shear has been discussed as early as 1975 Hancock and Mackenzie (1976); Ramberg (1975). To construct Mohr's circle, first the points $\{F_{11}, -F_{21}\}$ and $\{F_{22}, F_{12}\}$ (Fig. 7), which are the components of the deformation gradient $F$ , are drawn in a cartesian coordinate system. Both of these points lie on a circle. With the components of $F$ the radius R of the circle and the center of the circle on $\{S, Q\}$ can be calculated. We can find the rigid body rotation indicated by $\beta$. For pure shear, there is no rotation and $\beta$ is 0. The reader is referred to Electronic Supplementary Material 3 for an animated explanation for the construction of Mohr's circle of strain.

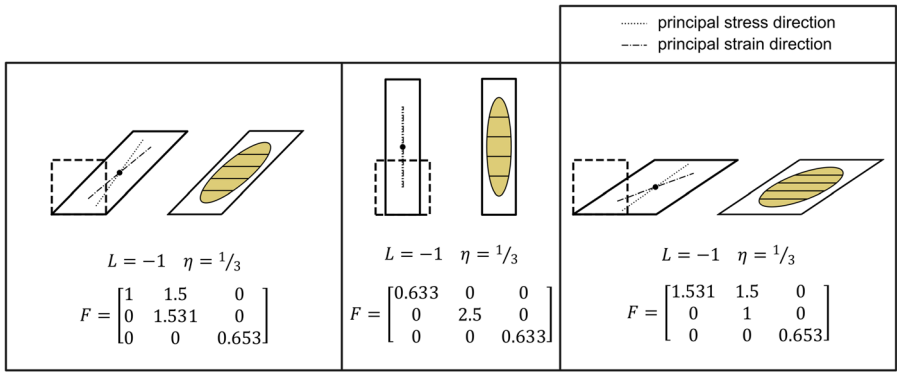


**Fig. 6** Three stress states described by $L_\sigma = -1$ and $\eta_\sigma = 0.333$ resulting from different deformation gradients with a von Mises material

It is important to note that two strain axes, which are 90° apart on the deformed element, are located 180° apart on Mohr's circle. This is called the double angles method. At the beginning of the deformation, the circle is oriented so that the horizontal line is parallel to the instantaneous stretch axis (ISA).

$$F = \begin{bmatrix} F_{11} & F_{12} & 0 \\ 0 & F_{22} & 0 \\ 0 & 0 & \frac{1}{F_{11} \cdot F_{22}} \end{bmatrix} \tag{16}$$

Mohr's circle of strain provides an easy and fast way to assess, whether the deformation is simple shear, general shear or pure shear. There is a number which serves to distinguish simple shear, general shear and pure shear. This number is called kinematic vorticity number and is defined as

$$W_k = \frac{Q}{R} \tag{17}$$

Depending on the value of the vorticity number, the deformation is categorized as $W_k = 0$: pure shear, $0 < W_k < 1$: general shear or $W_k = 1$: simple shear. We will introduce a new parameter to describe the stretch/shear ratio of elongation. The parameter $f_r$ appears in one of the diagonal entries of the deformation gradient. For simple shear superimposed with perpendicular uniaxial stretch $F_{11}$ is 1 (Eq. 18), for simple shear superimposed with parallel uniaxial stretch $F_{22}$ is 1 (Eq. 19).

$$F_{11} = 1 \text{ and } F_{22} = 1 + f_r \cdot v_0 \cdot dt \tag{18}$$

$$F_{11} = 1 + f_r \cdot v_0 \cdot dt \text{ and } F_{22} = 1 \tag{19}$$

The values of principal stretch can be calculated from geometric relationships. The principal stretches in the xy-plane can be calculated as $e_1 = T + R$ and $e_2 = T - R$. These stretch values can be directly converted to natural strains by taking their logarithm.

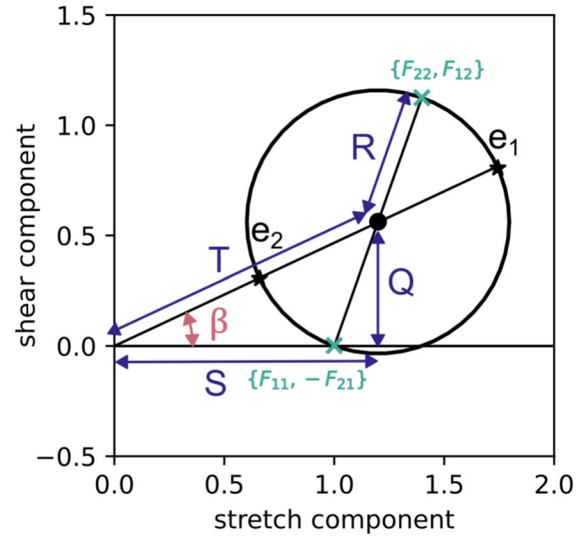


**Fig. 7** Mohr's circle for strains constructed from deformation gradient

Therefore, the principal strains are $\varepsilon_1 = log(e_1)$ and $\varepsilon_2 = log(e_2)$. It should be noted that even though we are not looking at plane strain, we are still using a 2D representation of Mohr's circle. We assume that any rotation taking place is happening in the xy-plane. While the strain in z-direction varies, due to incompressibility it is always uniquely related to the x and y values. The deformation in the z-direction results from the deformations given in x and y-direction. The indicators for simple shear are $W_k$ and/or $\beta$. These values appear in Mohr's circle of strain because the deformation gradient is asymmetric.

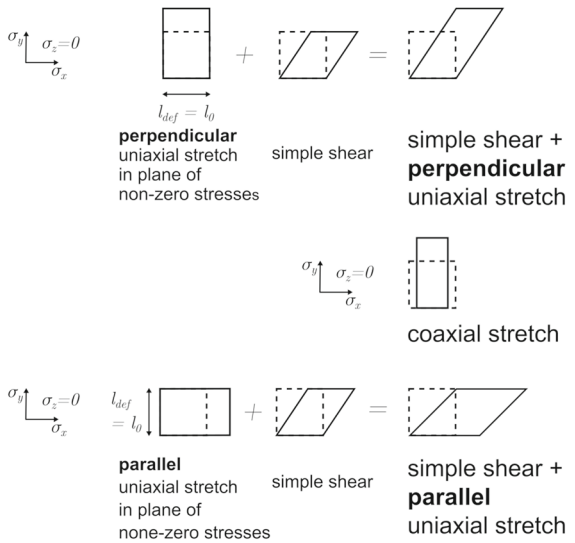


**Fig. 8** Nomenclature for different loading cases

## 2.5 Scope of stress states

The distinction between simple shear and coaxial stretch is relevant for various 3D stress states. To concisely present the key findings, the scope of this study is reduced to a subset of 2D stress states. In this study all cases which are discussed satisfy the following conditions:

- Constant volume / Incompressibility

$$\begin{aligned} \left(1+\varepsilon_{1,eng}\right)\left(1+\varepsilon_{2,eng}\right)\left(1+\varepsilon_{3,eng}\right) &= 1 \\ \varepsilon_{1,true}+\varepsilon_{2,true}+\varepsilon_{3,true} &= 0 \end{aligned} \tag{20}$$

- Plane stress condition

$$\sigma = \begin{bmatrix} \sigma_{11} & \sigma_{12} & 0 \\ \sigma_{12} & \sigma_{22} & 0 \\ 0 & 0 & 0 \end{bmatrix} \tag{21}$$

$$\xi_\sigma = -\frac{27}{2}\eta_\sigma\left(\eta_\sigma{}^2 - \frac{1}{3}\right) \tag{22}$$

- Superposition of simple shear with uniaxial stretch in the plane of non-zero stresses, i.e. the length of one side remains constant ($l_{def} = l_0$) (Fig. 8)
- The loading is proportional, i.e. $L_\sigma$ and $\eta_\sigma$ remain constant during deformation
- An elastoplastic von Mises material is assumed

Eq. (22) was derived by Bai and Wierzbicki (2008) and relates Lode parameter and triaxiality for plane stress condition. The material is assumed to be isotropic and behave according to a von Mises material.

**Table 1** Swift-Voce parameters for DP600 Schuster et al. (2024)

| | $A$ | $\varepsilon_0$ | $n$ | $k_0$ | $Q$ | $\beta_0$ | $\alpha$ |
|---|---|---|---|---|---|---|---|
| DP600 | 1045 | 0.001 | 0.36 | 797 | 418 | 43 | 0.64 |

## 2.6 Finite Element Simulation

A set of one-element finite element simulations is presented to validate the theoretical considerations. A dual-phase steel with an ultimate tensile yield strength of 600 MPa is a common steel grade found in the automotive industry and serves as an example. The considerations hold true for any other ductile material. The elastoplastic material behavior is described by a Swift-Voce relationship (Eq. 23). The parameters for DP600 are found in Table 1.

$$\begin{aligned} \sigma_{S-V} &= \alpha \cdot A\left(\varepsilon_0+\varepsilon_p\right)^n \\ &+ (1-\alpha)\cdot\left(k_0+Q(1-e^{-\beta_0\varepsilon_p})\right) \end{aligned} \tag{23}$$

The first addend in Eq. (23) contains the Swift parameters $A, \varepsilon_0, n$ , the second addend contains the Voce parameters $k_0$, $Q$, $\beta_0$. Parameter $\alpha$ describes how much each addend contributes to $\sigma_{S-V}$. These parameters are material dependent. One-element tests are set up to calculate variations of proportional loading for different $L_\sigma, \eta_\sigma$ pairs. The edge lengths of the elements are 1 mm. Elements with reduced integration of type C3D8R were used. The solver is ABAQUS 2020/Explicit.

Fig. 9 shows the node numbering and the coordinate system for the one element tests. Depending on the stress state, different velocities for different directions are applied to the nodes. The node numbered "1" is always fixed in space.

For a material defined through the *PLASTIC keyword in ABAQUS/Explicit, the calculation of stress components is based on the Jaumann rate of change of Kirchhoff stress. This algorithm splits the stress rate into a sum of a corotational rate and a rotational rate. For large deformations with rotation of the material this can lead to errors in the stress output Butcher and Abedini (2017); Bažant and Vorel (2014) . For an estimation of the error the results of normal stress and shear stress of a cube under simple shear with the DP600 material are shown in Fig. 10. The expected value for normal stress is zero but is calculated as about 5 MPa at an effective plastic strain of 0.8. This can be considered negligible compared to the shear stress which is about 600 MPa. Larger errors might occur if a VUMAT is

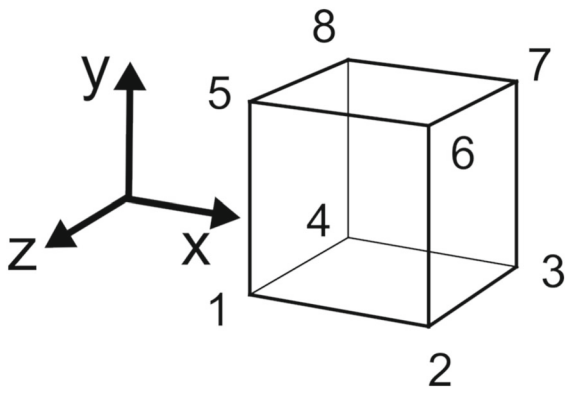


**Fig. 9** Definition of coordinate system and node numbering for one element tests

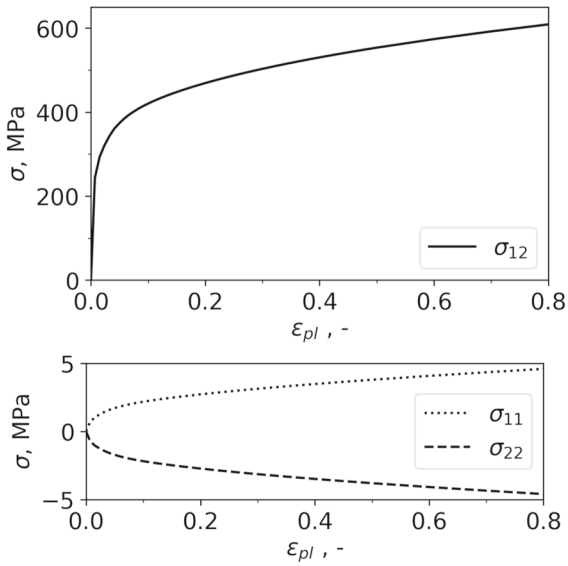


**Fig. 10** Results of shear stress (top) and normal stresses (bottom) for a simple shear deformation with DP600 showing inaccuracies caused by Jaumann rate algorithm

employed, which uses the Green-Naghdi algorithm. In this study however, all simulations are performed with the built-in plasticity model of ABAQUS/Explicit.

## 3 Results

We will look at how simple shear affects the results of the Lode parameter and triaxiality when these values are defined in stress space or strain space. Then we will derive a method to retrieve simple shear information from finite element results. This method uses the fact, that the principal axes of strain and stress do not remain colinear with increasing deformation.

### 3.1 Superposition of simple shear and tension and the effect on Lode angle and triaxiality

As we have seen, different deformations can lead to identical value pairs of Lode $L_\sigma$ and triaxiality $\eta_\sigma$, which suggests that the stress states are identical (Fig. 6). The goal is to find a measure that makes it possible to reconstruct the deformation gradient when simple shear is superposed with uniaxial stretch in the plane of non-zero stresses. We know that in the presence of simple shear, the deformation is rotational. This means that the directions of the principal strain and stress axis diverge. For coaxial stretch, both eigenvectors of strain and stress tensor stay colinear, while for superposed simple shear and uniaxial stretch, the eigenvectors diverge. We can use this angular difference to give us information about simple shear. This approach still works when the element moves during loading. The deformation gradient can be recovered with this approach, even when additional rigid body rotation in the absence of deformation occurs. The offset between principal strain axis and principal stress axis is a direct result of simple shear. We will refer to this offset as $\Delta\alpha$.

### 3.2 Offset between principal stress and principal strain axis reveals simple shear

Fig. 11 shows the evolution of $\Delta\alpha$, $L_\sigma$ and $L_\varepsilon$ for a cubic element, which was deformed with a superposition of simple shear with perpendicular stretch with a stretch/shear elongation ratio of $f_r = 0.707$. To achieve this deformation the nodes numbered 5,6,7 and 8 were displaced in positive y-direction. Simultaneously, nodes 6 and 7 were also displaced in x-direction. For the volume to remain constant, nodes 3,4,7 and 8 were allowed to move in z-direciton. We can see that the Lode parameter $L_\sigma$ calculated from principal stress (Eq. 7) and the Lode parameter $L_\varepsilon$ calculated from principal strain increments (Eq. 8) differ. While the Lode parameter $L_\sigma$ remains constant, the Lode parameter $L_\varepsilon$ increases as the deformation of the element progresses. This is a result of the principal axes of strain and stress not remaining colinear. All stress cases, where these

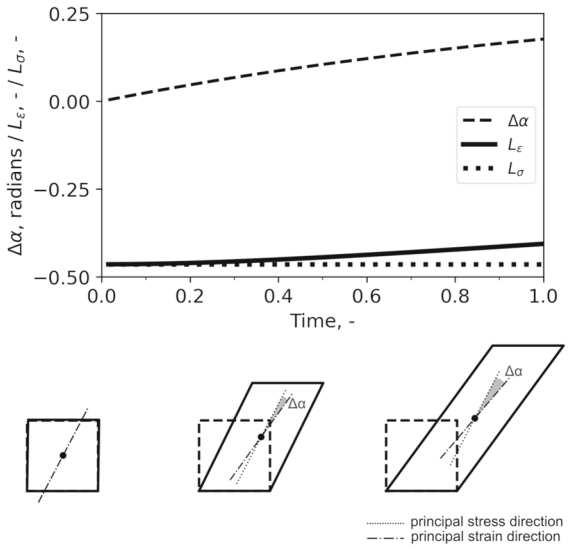


**Fig. 11** Evolution of deformation resulting in an offset between principal axes

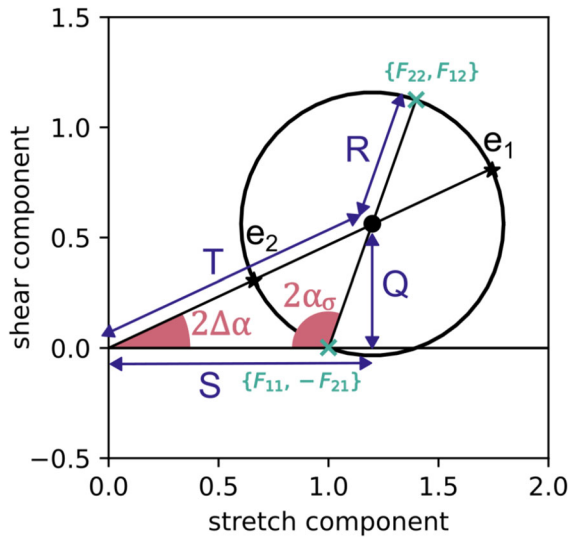


**Fig. 12** Evolution of deformation resulting in an offset between principal axes

two axes remain colinear have identical values for $L_\sigma$ and $L_\varepsilon$. Simple shear is the reason why the two axes diverge and therefore the reason we see a difference in Lode parameters $L_\sigma$ and $L_\varepsilon$. In conclusion, the difference between principal stress and principal strain axis $\Delta\alpha$ reveals the presence of simple shear.

While we can now distinguish a case with and without simple shear, information about whether the superposed stretch is in parallel or perpendicular to the shear direction cannot be recovered with only $\Delta\alpha$. The angular difference $\Delta\alpha$ turns out to be the same for both variations (superpositions with parallel / perpendicular stretch). Whether we are dealing with parallel or perpendicular stretch is contained in the absolute value of the principal stress axis direction $\alpha_\sigma$. The angle is measured as the angular distance from the x-axis, which is the horizontal axis in our case. An absolute value of $\alpha_\sigma$ lower than 45° means that the superposed stretch is applied along the x-axis parallel to the shear direction, an absolute value higher than 45° means that the superposed stretch is applied along the y-axis, perpendicular to the shear direction. There is a geometrical interpretation of the deformation gradient as we have seen in Mohr's circle Section 2.4. This will help to interpret why the value of Lode parameter changes in strain space but not in stress space. It will be discussed in the next section.

### 3.3 Identifying offset $\Delta\alpha$ in Mohr's circle for strains

From geometric dependencies in Mohr's circle Fig. 12, we can conclude that the angle $\alpha_\sigma$ can be calculated from the stretch/shear elongation ratio $f_r$. This relationship holds true when the superposition is comprised of simple shear and uniaxial stretch. For superposition with perpendicular stretch, we set $F_{11}$ to 1 in the deformation gradient Eq. (16). For superposition with parallel stretch, we set $F_{22}$ to 1. The value for $F_{21}$ is 0 in both cases. The resulting equations for $\alpha_\sigma$ are shown in Eq. (24). For simple shear without stretch, i.e. $f_r = 0$, the principal direction of stress is 45°, because the second addend vanishes. For perpendicular stretch the sign of the second term is positive, for parallel tension the sign of the second addend is negative. In 3.5 we will calculate $f_r$ for arbitrary values of $L_\sigma$ and give specific values $f_r$ for stress states of particular interest.

$$\alpha_{I\sigma A} = \begin{cases} \frac{\pi}{4} - 0.5 \arctan\left(f_r\right), & \text{simple shear} \\ & \textbf{+ parallel stretch} \\ \frac{\pi}{4} + 0.5 \arctan\left(f_r\right), & \text{simple shear} \\ & \textbf{+ perpendicular} \\ & \textbf{stretch} \end{cases} \tag{24}$$

We will call this angle the angle of the instantaneous stress axis $\alpha_{I\sigma A}$, in analogy with the instantaneous stretch axis used in geology. The angle of instan-

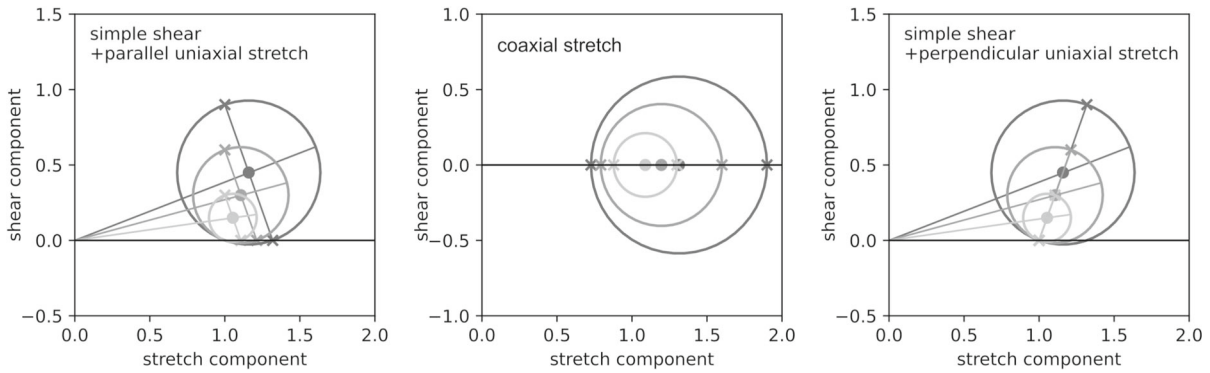


**Fig. 13** Evolution of deformation for simple shear + parallel stretch (left), coaxial stretch (middle) and simple shear + perpendicular stretch (right).

taneous stress axis $\alpha_{I\sigma A}$ describes the angle between the shear direction and the principal stress direction. The direction of principal stress $\alpha_\sigma$ / $\alpha_{I\sigma A}$ remains constant during the deformation (Fig. 13), while the direction of principal strain $\alpha_\varepsilon$ varies. As the deformation progresses the angle of principal strain direction decreases, while the difference between the two principal axes $\Delta\alpha$ increases. The deformation gradient has an asymmetric entry that moves the center of Mohr's circle in the vertical direction, which informs the value of kinematic vorticity $W_k$ and thus gives information about simple shear.

### 3.4 Relationship between $\Delta\alpha$ and stress state

We have seen that the Lode parameter $L_\sigma$ calculated from Eq. (7) remains constant and so does the angle of the principal stress direction $\alpha_\sigma$. In this section, we will aim to find a relationship between $L_\sigma$ and $\alpha_\sigma$, which will then facilitate giving us a value for the stretch/shear elongation ratio $f_r$ to set an arbitrary stress state. Next, we will define a relationship between $L_\varepsilon$ and $\alpha_\sigma$, $\Delta\alpha$ which will provide the link between Lode parameter defined from stress values and Lode parameter defined from strain values. We know that $L_\sigma$ and $L_\varepsilon$ are equal in the beginning and only diverge as the deformation progresses. We use this fact to modify Eq. (8). With a vanishingly small time increment and a constant value of $L_\sigma$ the equation can be written as follows

$$L_\sigma = \frac{3\,\varepsilon_2}{\varepsilon_1 - \varepsilon_3} \tag{25}$$

Since we are assuming an incompressible material, we can write the true strain values in relation to the stretches with $\varepsilon_1 = \log(e_{1\prime})$, $\varepsilon_2 = \log(e_{2\prime})$, $\varepsilon_3 = \log\left(\frac{1}{e_{1\prime}\cdot e_{2\prime}}\right)$. Applying logarithmic rules, the equation can be written as

$$L_\sigma = \frac{3\,\log(e_2)}{\log\left({e_1}^2\cdot e_2\right)} \tag{26}$$

In 2.5 we have narrowed the scope of our study to a subset of superposed deformations. The next simplifications therefore only apply to superposed simple shear with uniaxial stretch in the plane of non-zero stresses. From Mohr's circle we can use $e_{1\prime} = T + R$, $e_{2\prime} = T - R$ and $e_{3\prime} = \frac{1}{e_1\cdot e_2}$. We are using the indices $1\prime, 2\prime, 3\prime$ because these stretch values are not ordered in magnitude. The order of magnitude is dependent on the shear/stretch elongation ratio. From Mohr's circle, we can substitute T and R and introduce $\alpha_\sigma$, $f_r$ and $b$ into the equation. The value of $b$ is the shear deformation and equal to the entry $F_{12}$ in the deformation gradient (Eq. 12). At the beginning of deformation $b$ is vanishingly small. By determining the limit of the equation with $b \to 0$ we arrive at

- $T + R > \frac{1}{T^2 - R^2} > T - R$ and triaxiality $\eta_\sigma \leq \frac{1}{3}$ and shear ratio $f_r \leq \frac{1}{2\sqrt{2}} \approx 0.354$

$$L_\sigma = -3 \cdot f_r \cdot \sin(2\alpha_\sigma) \tag{27}$$

$$L_\sigma = -\frac{3 \cdot f_r}{\sqrt{{f_r}^2 + 1}} \tag{28}$$

- $T + R > T - R > \frac{1}{T^2 - R^2}$ and triaxiality $\eta_\sigma \geq \frac{1}{3}$ and shear ratio $f_r \geq \frac{1}{2\sqrt{2}} \approx 0.354$

$$L_\sigma = \frac{-3\,(1 - f_r \cdot \sin(2\alpha_\sigma))}{3 \cdot f_r \cdot \sin(2\alpha_\sigma) + 1} \tag{29}$$

$$L_\sigma = \frac{3 \cdot f_r - 3 \cdot \sqrt{{f_r}^2 + 1}}{\sqrt{{f_r}^2 + 1} + 3 \cdot f_r} \tag{30}$$

These equations meet at $f_r = \frac{1}{2\sqrt{2}} \approx 0.354$ which results in a Lode parameter of $L_\sigma = -1$.

To get the Lode parameter $L_\varepsilon$ depending on $\alpha_\sigma$ and $\Delta\alpha$ we go back to Eq. (8) and define the strain increments depending on the change in angular difference between principal strain and stress axis. Using stretch definitions and employing logarithmic rules we arrive at

$$L_\varepsilon = \frac{3 \log\left(\frac{e_{2,i}}{e_{2,i-1}}\right)}{\log\left(\left(\frac{e_{1,i}}{e_{1,i-1}}\right)^2 \cdot \frac{e_{2,i}}{e_{2,i-1}}\right)} \tag{31}$$

with

$$\frac{e_{1,i}}{e_{1,i-1}} = \left(\frac{\csc(2\Delta\alpha_i) + \csc(2\alpha_\sigma)}{\csc(2\Delta\alpha_{i-1}) + \csc(2\alpha_\sigma)}\right)\left(\frac{t_i}{t_{i-1}}\right) \tag{32}$$

and

$$\left(\frac{t_{i-1}}{t_i}\right) = \frac{\cot(2\Delta\alpha_i) - \cot(2\alpha_\sigma)}{\cot(2\Delta\alpha_{i-1}) - \cot(2\alpha_\sigma)} \tag{33}$$

Again, we distinguish two cases, since the equation for the second principal strain differs

- $T + R > \frac{1}{T^2 - R^2} > T - R$ and triaxiality $\eta_\sigma \leq \frac{1}{3}$ and shear ratio $f_r \leq \frac{1}{2\sqrt{2}} \approx 0.354$

$$\frac{e_{2,i}}{e_{2,i-1}} = \left(\frac{\csc^2(2\Delta\alpha_{i-1}) - \csc^2(2\alpha_\sigma)}{\csc^2(2\Delta\alpha_i) - \csc^2(2\alpha_\sigma)}\right)\left(\frac{t_{i-1}}{t_i}\right)^2 \tag{34}$$

- $T + R > T - R > \frac{1}{T^2 - R^2}$ and triaxiality $\eta_\sigma \geq \frac{1}{3}$ and shear ratio $f_r \geq \frac{1}{2\sqrt{2}} \approx 0.354$

$$\frac{e_{2,i}}{e_{2,i-1}} = \left(\frac{\csc(2\Delta\alpha_i) - \csc(2\alpha_\sigma)}{\csc(2\Delta\alpha_{i-1}) - \csc(2\alpha_\sigma)}\right)\left(\frac{t_i}{t_{i-1}}\right) \tag{35}$$

As we can see the Lode parameter $L_\varepsilon$ only depends on the angles of principal stress direction $\alpha_\sigma$ and the angular difference $\Delta\alpha$ between principal stress and strain direction. This difference $\Delta\alpha = \alpha_\sigma - \alpha_\varepsilon$ increases with shear deformation. We will validate these equations with finite element simulations in Section 2.6.

With Eq. (28) and Eq. (30) it is possible to calculate the exact values of $f_r$ for a specific value pair $L_\sigma, \eta_\sigma$ with triaxiality calculated for plane stress from Eq. (22). A variety of different stress states with their corresponding $L_\sigma$, $\eta_\sigma$, $f_r$ values is shown in Fig. 2. We can arrive at the same pair of $L_\sigma, \eta_\sigma$ for different deformations in the range of $L_\sigma, \eta_\sigma = (0, 0)$ and $L_\sigma, \eta_\sigma = (0, \frac{1}{\sqrt{3}})$.

### 3.5 Setting up one-element tests for specific stress states

In this section we will present boundary conditions to create one-element tests for specific stress states. The equations to create velocity curves for the moving nodes to obtain specific stress states with and without superposed simple shear are presented. Then we calculate the stretch / shear elongation ratio $f_r$ for arbitrary stress states defined by Lode parameter $L_\sigma$ and triaxiality $\eta_\sigma$.

#### *3.5.1 Coaxial stretch without simple shear*

In this subsection we are working with coaxial stretch without a shear component, therefore, the definitions of $L_\varepsilon$ and $L_\sigma$ are interchangeable. We choose the y-direction to apply a constant velocity $v_0$. The resulting displacement in y-direction is straightforward with $dy = v_0 \cdot dt$.

The stretch in x-direction is derived from the relationship between true strain and engineering strain, which have a logarithmic relationship. Depending on whether we want a triaxiality of less than one-third or higher than one-third this gives us the following equations.

$$dx = \begin{cases} (1+dy)^{\frac{L_\sigma+3}{L_\sigma-3}} - 1 & , \ \eta \leq \frac{1}{3} \\ (1+dy)^{-\frac{L_\sigma+3}{L_\sigma-3}-1} - 1 & , \ \eta \geq \frac{1}{3} \end{cases} \tag{36}$$

So, for the prescribed motion we can calculate the velocity in x-direction as.

$$v_x(L,\ dt) = \frac{dx}{dt} \tag{37}$$

The velocity curves $v_x(L,\ dt)$ can be calculated and entered in tabular form into ABAQUS. The velocity is prescribed on nodes 2,3,6,7 (Fig. 14).

#### *3.5.2 Simple shear superposed with uniaxial stretch*

With equations established in Section 3.4 namely Eq. (28) and Eq. (30), we can calculate the stretch/shear elongation ratio $f_r$ for a desired value of Lode parameter $L_\sigma$. We rearrange these equations and obtain

$$f_r(L_\sigma) = \begin{cases} -\frac{L_\sigma}{\sqrt{9 - {L_\sigma}^2}} & , \ \eta \leq \frac{1}{3} \\ \sqrt{\frac{-{L_\sigma}^2 - 6 \cdot L_\sigma - 9}{-8 \cdot {L_\sigma}^2 + 24 \cdot L_\sigma}} & , \ \eta \geq \frac{1}{3} \end{cases} \tag{38}$$

with $-1 \leq L_\sigma \leq 0$.

$$v_\gamma = f_r \cdot v_0 \tag{39}$$

**Table 2** The deformed elements in each column depict a stress state with the same pair of Lode parameter $L_\sigma$ and triaxiality $\eta_\sigma$

| | pure/simple shear | | uniaxial tension | | plane strain | |
|---|---|---|---|---|---|---|
| stretch/shear ratio $f_r$ | 0 | $\sqrt{\frac{3\sqrt{3}-5}{8}}$ | $\frac{1}{2\sqrt{2}}$ | $\frac{1}{\sqrt{2}}$ | $\infty$ | |
| Lode parameter $L_\sigma$ | 0 | $3-2\sqrt{3}$ | $-1$ | $3-2\sqrt{3}$ | 0 | |
| Lode parameter $\xi_\sigma$ | 0 | $\frac{1}{\sqrt{2}}$ | 1 | $\frac{1}{\sqrt{2}}$ | 0 | |
| Lode angle $\theta_\sigma$ | $\frac{\pi}{6}$ | $\frac{\pi}{12}$ | 0 | $\frac{\pi}{12}$ | $\frac{\pi}{6}$ | |
| triaxiality $\eta_\sigma$ | 0 | $\frac{-1+\sqrt{3}}{3\sqrt{2}}$ | $\frac{1}{3}$ | $\frac{\sqrt{2}}{3}$ | $\frac{1}{\sqrt{3}}$ | |
| simple shear + **perpendicular** stretch | 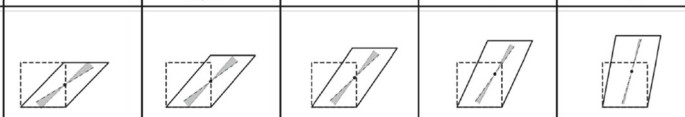 | | | | | principal stress axis<br>principal strain axis<br>undeformed<br>deformed |
| coaxial stretch | 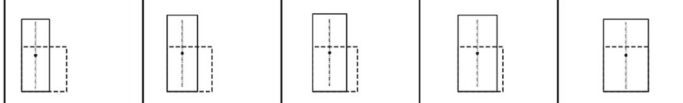 | | | | | |
| simple shear + **parallel** stretch | 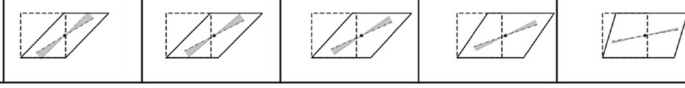 | | | | | |

Depending on whether the uniaxial stretch is superposed in parallel or perpendicular, the velocity is prescribed on different nodes (Fig. 14). The analytical values for distinct $L_\sigma$, $\eta_\sigma$ pairs of five different stress states are shown in 2. With sufficient accuracy the corresponding values for $f_r$ can be approximated with $f_r\,(L_\sigma, \eta_\sigma) = 0.\,/\,0.157\,/\,0.354\,/\,0.707\,/\,2.$

### 3.6 Validation with Finite Element results

One-element tests have been carried out in ABAQUS/Explicit with the boundary conditions described in Fig. 14. There are five distinctive stress states. Each of these stress states is realized by utilizing three different variations of deformation. One variation uses simple shear superposed with parallel stretch, the second uses simple shear superposed with perpendicular stretch and the third uses coaxial stretch without simple shear (Fig. 2). We will compare the finite element results with analytical results to validate the equations and extract more information regarding different descriptions of stress states involving simple shear.

The input file for the one-element tests is available as Electronic Supplementary Material 4. The values for the logarithmic strain components, which are labeled "LE" and the stress components, which are labeled "S" are directly output from the ABAQUS solver. All other values (principal values, angles, Lode parameters) are calculated in post-processing. For each time step the principal strain increment was calculated. Those increments were sorted by magnitude and used in Eq. 8 to get the Lode parameter $L_\varepsilon$ of the simulation.

The analytical solution was obtained as described in Section 3.4. The angles of principal stress direction $\alpha_\sigma$ were calculated with Eq. (24) for a given stretch/shear elongation ratio $f_r$. The difference in principal angles was calculated by polar decomposition of the deformation gradient, which gives the rigid body rotation. For our cases the rigid body rotation angle is identical to the difference in principal value directions $\Delta\alpha$. The curves of the analytical solution and numerical solution coincide (Fig. 15, Fig. 16), which gives validity to the developed equations in this study (Section 3.4).

| | Fixed DOFs | Fixed nodes | Moving nodes | Prescribed motion |
|---|---|---|---|---|
| simple shear + **perpendicular** stretch | 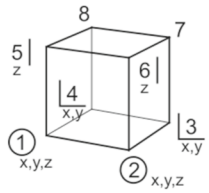 | **x=0:** 1, 2, 3, 4<br>**y=0:** 1, 2, 3, 4<br>**z=0:** 1, 2, 5, 6 | 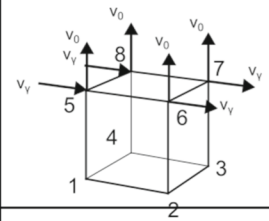 | **$v_0$:** 5,6,7,8<br>**$v_\gamma = f_r\, v_0$:** 5,6,7,8 |
| coaxial stretch | 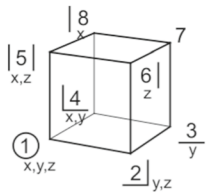 | **x=0:** 1, 4, 5, 8<br>**y=0:** 1, 2, 3, 4<br>**z=0:** 1, 2, 5, 6 | 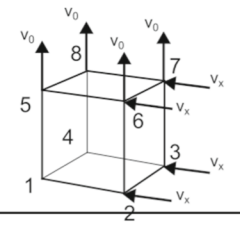 | **$v_x$(dt) with Eq.(36):**<br>5, 6, 7, 8 |
| simple shear + **parallel** stretch | 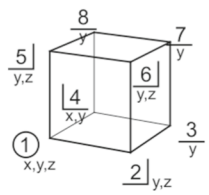 | **x=0:** 1, 4<br>**y=0:** all nodes<br>**z=0:** 1, 2, 5, 6 | 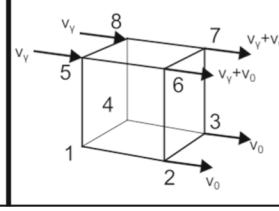 | **$v_0$:** 2,3<br>**$v_\gamma = f_r\, v_0$:** 5, 8<br>**$v_\gamma + v_0$:** 6,7 |

**Fig. 14** Boundary conditions to create specific stress states

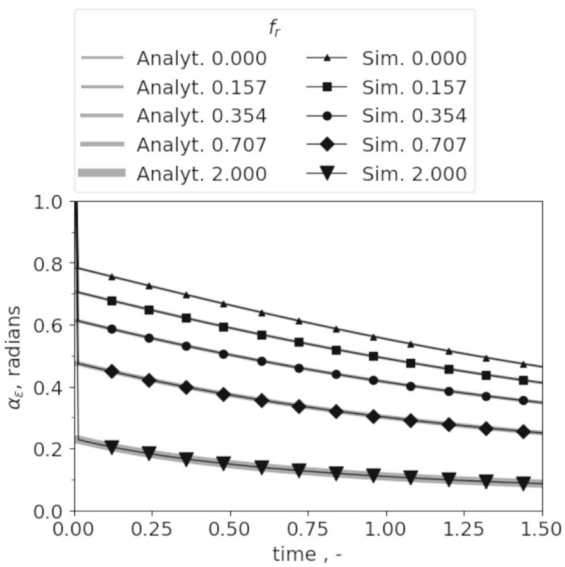


**Fig. 15** The evolution of principal strain direction $\alpha_\varepsilon$ for different stretch/shear ratios $f_r$ with increasing deformation

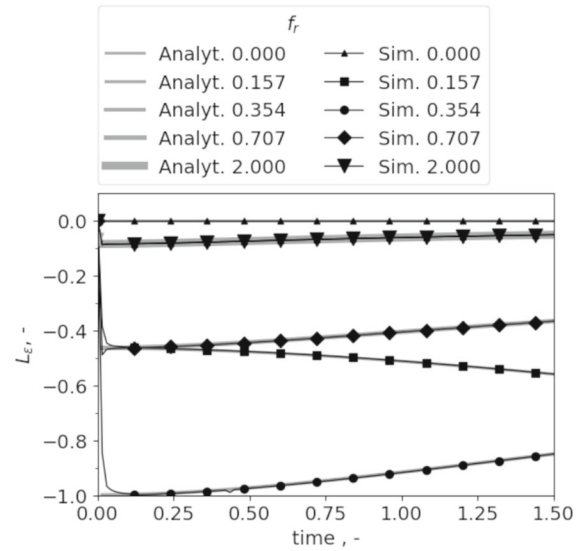


**Fig. 16** The evolution of Lode parameter $L_\varepsilon$ for different stretch/shear ratios $f_r$ with increasing deformation

Remember that the Lode parameter also describes the ratio of stretches in the three principal directions. The Lode parameter $L_\varepsilon$ reveals that the relationship between the three principal strains changes during deformation when simple shear is present. This change is easily interpreted by the rotation of the axis of principal strains. But from Lode angle defined by principal stresses $L_\sigma$ this change cannot be detected. For an anisotropic material however, the relative change in principal strain magnitudes can have significant implications. Note that for simple shear superposed with uniaxial stretch, the difference in angles $\Delta\alpha$ and the angle in principal stress direction $\alpha_\sigma$ are sufficient to calculate Lode parameter $L_\varepsilon$. This is valid within the scope of our assumptions (Section 2.5).

A more familiar visualization of the stress state during loading is strain paths. The strain path shows the value of triaxiality and/or Lode parameter against the equivalent plastic strain. If the strain path is a vertical line the loading is called proportional. We have set up all one-element tests to have proportional loading in stress space. Since the elastic part is very small and we want to get a visualization that is not dependent on the material, we use the effective strain calculated from logarithmic strains. In Fig. 17 and Fig. 18 both strain paths in stress space and in strain space are presented. The triaxiality calculated from principal strains $\eta_\sigma$ is ouput by ABAQUS directly and is equal to the value resulting from Eq. (22). The triaxiality $\eta_\varepsilon$ was calculated with Eq. (9). The strain paths are plotted until an equivalent strain value of 0.76 is reached.

The individual strain paths in Fig. 17 and Fig. 18 are discussed below.

- $L_\sigma, \eta_\sigma = (0, 0)$
  The strain paths for simple shear and coaxial stretch are identical for the definition in stress space as well as in strain space. Here it is interesting to point out, that the difference in angles between principal strain and stress direction is the largest for simple shear. But that does not cause a shift in the value of $\eta_\varepsilon$. This is simply because the second principal strain $\varepsilon_2$ is always zero, which results in $L_\varepsilon$ remaining zero throughout the deformation. That does not mean that these stress states are identical. Because of the rotation of the principal strain axis, the rate at which equivalent strain and equivalent stress will grow in relation to each other will differ.
- $L_\sigma, \eta_\sigma = (3 - 2\sqrt{3}, (-1 + \sqrt{3})/(3\sqrt{2}))$ and $L_\sigma, \eta_\sigma = (3 - 2\sqrt{3}, \sqrt{2}/3)$
  The strain paths at $\eta_\sigma \approx 0.173$ and $\eta_\sigma \approx 0.471$ have the same value of $L_\sigma \approx -0.464$ and are discussed together. With increasing $\Delta\alpha$ the value of $\eta_\varepsilon$ increasingly differs from $\eta_\sigma$ when simple shear is involved. For $\eta_\sigma \approx 0.173$ / $f_r = 0.157$ the triaxiality $\eta_\varepsilon$ diverges faster than for $\eta_\sigma \approx 0.471$ / $f_r = 0.707$. The angular difference $\Delta\alpha$ also diverges faster for smaller triaxiality values than for higher triaxiality values.
- $L_\sigma, \eta_\sigma = (-1, \frac{1}{3})$
  We have discussed that during loading with $f_r = 0.354$ which corresponds to the stress state $L_\sigma, \eta_\sigma = (-1, \frac{1}{3})$ the ordering of $d\varepsilon_1 > d\varepsilon_2 > d\varepsilon_3$ changes midway and so does the ordering of the stresses. This leads to a discontinuity in the strain path with $\eta_\varepsilon$.
- $L_\sigma, \eta_\sigma = (0, \frac{1}{\sqrt{3}})$
  In Fig. 17 the strain path does not coincide with $\eta_\sigma = \frac{1}{\sqrt{3}}$ exactly. The value is about 0.561. Eq. (30) cannot reach $L_\sigma = 0$ exactly. The equation asymptotically approaches 0 but never reaches it. However, a value of $f_r = 2.0$ does provide a stress state close to plane strain.

All parameters used to describe the stress state, i.e. $\Delta\alpha$ and triaxiality and Lode parameter can be described as angular values (Section 2.1). Since we are considering the ordering of principal values, a lot of case distinctions need to be considered in the different equations for the stress state parameters. It remains an open question whether describing Lode parameter and triaxiality is a suitable framework to describe simple shear superposed with uniaxial stretch. Even with Lode parameter and triaxiality defined in strain space, simple shear $L_\sigma, \eta_\sigma = (0, 0)$ cannot be distinguished from coaxial stretch with $L_\sigma, \eta_\sigma = (0, 0)$ although they have the largest difference in principal strain and principal stress direction $\Delta\alpha$. Irrespective of the presence of a shear component, the strain paths at $L_\sigma, \eta_\sigma = (0, 0)$ coincide.

### 3.7 FE results in a spherical coordinate system

As we have seen in Section 2.6, descriptions of stress states with Lode parameter / triaxiality do not provide a way to distinguish simple shear and pure shear stress

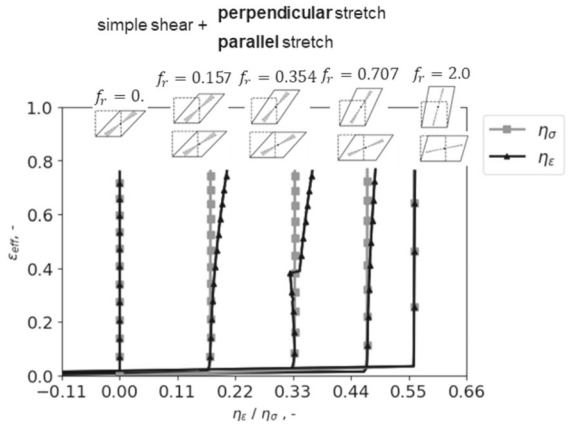


**Fig. 17** Strain paths for one element tests with simple shear superposed with parallel/perpendicular stretch

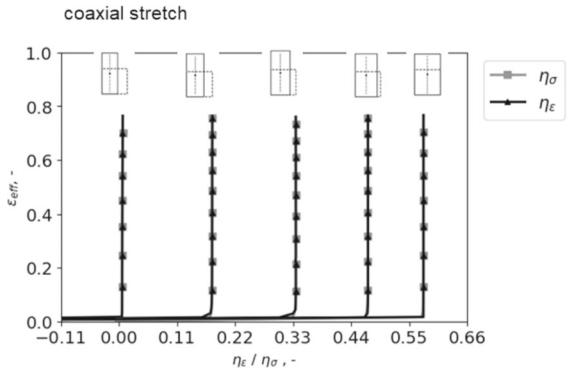


**Fig. 18** Strain paths for one element tests with coaxial stretch

states. A stress state description utilizing a spherical coordinate system as described in (Section 2.2) can overcome these shortcomings. The same strain paths resulting from the one-element tests in Fig. 2 were calculated depending on the shear and normal angle according to Eq. (10) and Eq. (11).

It was suggested that the shear angle $\psi_S$ can be used in combination with $\eta_\sigma$ for an isotropic material, but Fig. 19a shows that this description of stress states with $\eta_\sigma$, $\psi_S$ does not distinguish simple shear superposed with parallel stretch from simple shear superposed with perpendicular stretch. The strain paths for these stress states coincide. The stress state description with $\psi_S$, $\phi_N$ is more suitable. The strain paths for each one-element test appear as a distinct line in Fig. 19b. The shear angle $\psi_S$ is zero for one-element tests without superposed stretch. The shear angle increases with an increasing value of the stretch/shear elongation ratio

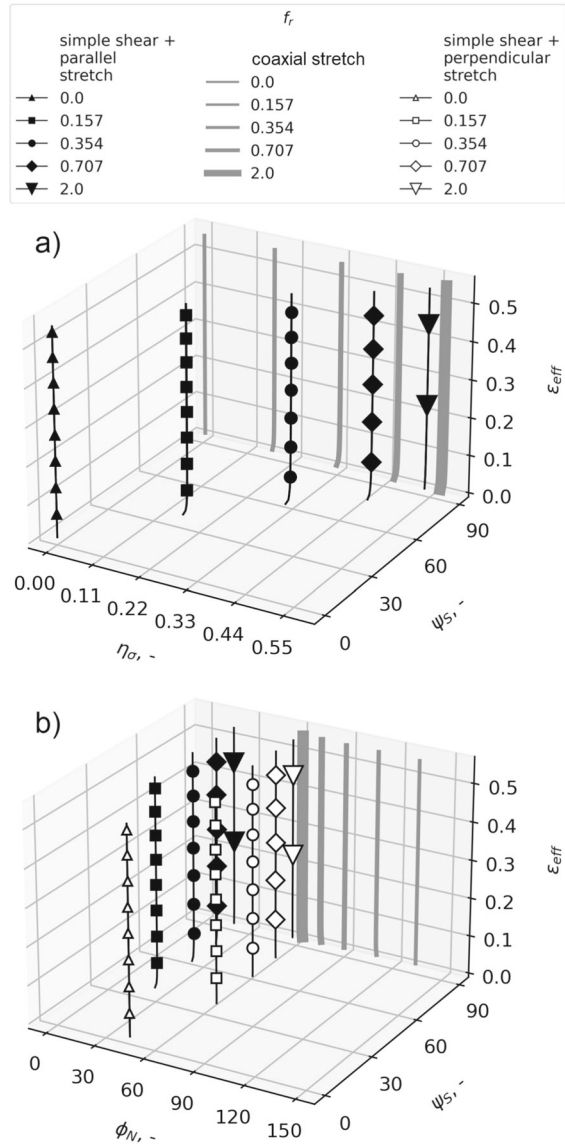


**Fig. 19** Strain paths for combined shear and coaxial stretch described by (a) $\Psi_S$, $\eta_\sigma$ and (b) $\Psi_S$, $\Phi_N$

$f_r$. In other words, the highest rate of increase in non-coaxiality occurs for $\psi_S = 0°$ and toward higher values of $\psi_S$ the stress state tends toward coaxiality. For a value of $\psi_S = 90°$ the deformation is coaxial and there is no component of simple shear. When simple shear is superposed with parallel stretch, the normal angle is $\phi_N \approx 26.5°$, when simple shear is superposed with perpendicular stretch the normal angle is $\phi_N \approx 63.4°$. The normal angle for simple shear is strictly speaking not defined. Any value of $\phi_N$ satisfies Eq. (10) when

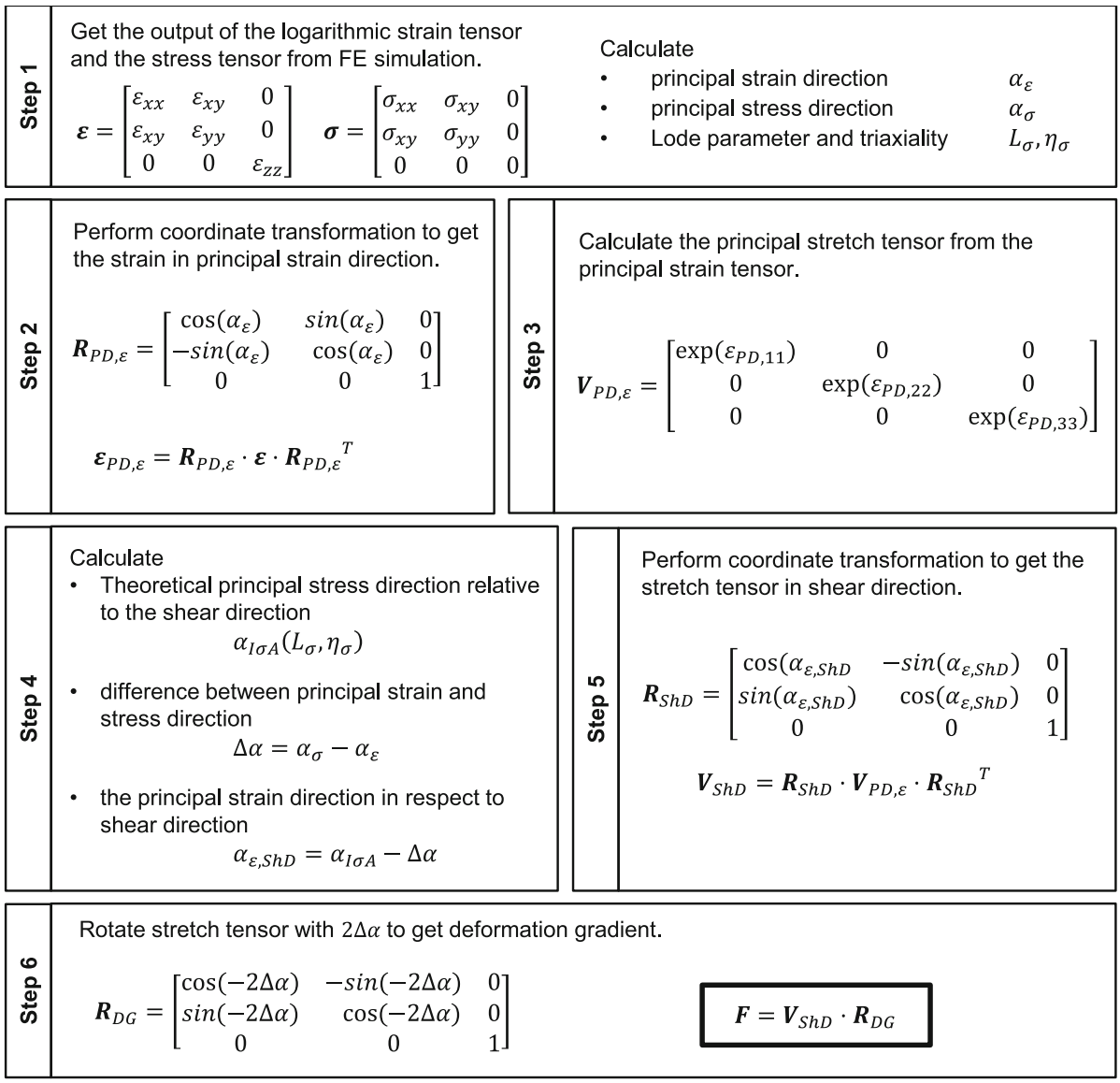


**Fig. 20** Steps for the reconstruction of a deformation gradient for a proportional loading

$\psi_S = 0°$. From the numerical simulation of the simple shear one-element test a value of $\phi_N \approx -45°$ resulted. The absolute value of $\phi_N$ is plotted in Fig. 19b for simple shear in order to keep consistency with the rest of the one-element tests.

A problem arises when the element is not oriented parallel to the shear direction. The Cauchy stress is defined in the global coordinate system and therefore any rigid body rotation of the element will make it impossible to use Eq. (10) and Eq. (11) directly. In the next section, we will show how to recover the angle that defines the shear direction by employing Eq. (24).

### 3.8 Reconstructing the shear direction from FE results

In the previous sections, we have clarified that simple shear can be interpreted as rigid body rotation and shows up as an off-diagonal entry in the deformation gradient. The Cauchy stress tensor and the logarithmic strain tensor, which are commonly used in FE soft-

ware as output results are symmetric and do not contain information about rigid body deformation and in consequence no information about simple shear. By combining information from stress and strain tensor, the deformation gradient and therefore information about simple shear can be recovered.

### *3.8.1 Proportional loading*

In the case of proportional loading, only the current values of the stress and strain tensor are needed to reconstruct the deformation gradient. Fig. 20 describes the necessary steps to calculate the deformation gradient. The theoretical angle of principal stress direction is calculated for the current triaxiality and Lode parameter. Since the angle of principal stress direction remains constant during proportional loading, this theoretical angle can be used to determine the direction of shear. The difference between the theoretical principal stress angle and the actual principal stress angle is equal to the inclination of the shear direction. This makes this process robust toward deformation with rigid body rotation.

For convenience, Equations (24,28,30) are rearranged, so that $\alpha_{I\sigma A}$ can be calculated directly from $L_\sigma$. Eq. (40) is valid for simple shear superposed with parallel stretch; Eq. (41) is valid for simple shear superposed with perpendicular stretch. The distinction between superposed parallel stretch and perpendicular is implemented by comparing the stress component in x and y direction. The stress component with the higher magnitude determines the direction of uniaxial stretch.

- simple shear + parallel stretch

$$\begin{aligned} \alpha_{I\sigma A} &= \frac{1}{2}\arccos\left(-\frac{L_\sigma}{3}\right), \eta \le \frac{1}{3} \\ \alpha_{I\sigma A} &= \frac{1}{2}\arccos\left(-\frac{-3-L_\sigma}{3\,(L_\sigma-1)}\right), \eta \ge \frac{1}{3} \end{aligned} \tag{40}$$

- simple shear + perpendicular stretch

$$\begin{aligned} \alpha_{I\sigma A} &= \frac{1}{2}\arccos\left(\frac{L_\sigma}{3}\right), \eta \le \frac{1}{3} \\ \alpha_{I\sigma A} &= \frac{1}{2}\arccos\left(-\frac{-3-L_\sigma}{3\,(1-L_\sigma)}\right), \eta \ge \frac{1}{3} \end{aligned} \tag{41}$$

### *3.8.2 Non-proportional loading*

An additional one-element test is calculated (Electronic Supplementary Material 5). This time the Lode parameter does not remain constant. The Lode parameter varies from 0 to -1 with $L_\sigma = -\sqrt{\frac{t}{t_{max}}}$. The resulting strain path is non-proportional. The steps are identical to the steps in Fig. 20 except for step 4, which is replaced by the step described in Fig. 21. For the calculation to work, it is assumed that $L_\sigma$ remains constant over an infinitesimal time step. For non-proportional loading the calculation of $f_{r,k}(L_{\sigma,k}, \eta_{\sigma,k})$ with Eq. (38) for the current Lode parameter / triaxiality pair is required. Additionally, the sum of $f_{r,k}$ needs to be calculated. The resulting value of $f_{r,sum}$ is needed to calculate the value of $\alpha_{I\sigma A}$, which is reached at time $t_k$.

The difference between $\alpha_{I\sigma A,k}$ calculated from the current value pair of $L_{\sigma,k}$, $\eta_{\sigma,k}$ and the angle of principal direction $\alpha_\sigma$ provides information about the angle of the shear direction. Therefore, this calculation is also robust against rigid body rotations.

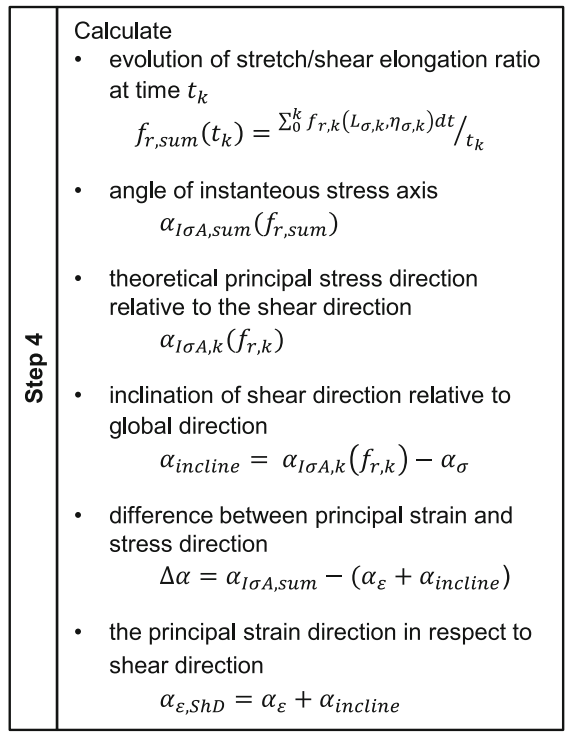


**Fig. 21** Modified Step 4 to account for non-proportional loading in recovering the deformation gradient

## 4 Conclusion

In this study, we looked at several stress state examples, which can be described by identical pairs of triaxiality and Lode parameter. We saw that with this widely used

description of stress states, it is not possible to distinguish stress states that involve simple shear. A method to identify simple shear for different stress states was presented. When simple shear is involved, the angle between principal stress axis and principal strain axis increases with progressing deformation. By using the difference in angles, we can identify the shear direction.

Describing the stress state with spherical coordinates allows us to decompose the stress state into shear and normal part. It requires an evaluation of the stress tensor oriented in alignment with the shear direction. This is usually not the case. By comparing the instantaneous stress axis to the principal stress axis the shear direction can be calculated. The present study provides the steps on how to reconstruct the shear direction and deformation gradient. These values can help to develop failure models that require stress and strain tensors to be oriented in alignment with the shear plane.

The results of the study should encourage the reader to consider stress states with simple shear superposed with coaxial stretch in the development and calibration of failure models. There is limited knowledge on how the presence of simple shear affects damage evolution. One way to study the effect would be by numerical simulation of representative volume elements (RVE) with voids. The present study provides boundary conditions to set up one-element tests with specific values of simple shear superposed with uniaxial stretch in the plane of non-zero stresses. These examples can be used to create RVEs.

While the scope of this study has been narrowed to only a certain range of stress states, it will be interesting to see how these considerations about identifying simple shear in various stress states can be expanded to biaxial stretch in the plane of non-zero stresses and stress states other than plane stress.

## Supplementary information

ESM 1: 2D Animation demonstrating coaxial and non-coaxial deformation of two unit cubes along identical strain paths

ESM 2: 3D Animation demonstrating coaxial and non-coaxial deformation of two unit cubes along identical strain paths

ESM 3: Animation demonstrating the construction of Mohr's circle

ESM 4: One-element tests Proportional

ESM 5: One-element tests Non proportional

ESM 6: ABAQUS input file for one-element tests with proportional loading

ESM 7: ABAQUS input file for one-element tests with non-proportional loading

**Acknowledgements** No funding was received to assist with the preparation of this manuscript.

**Funding** Open Access funding enabled and organized by Projekt DEAL.



## References

Anderson D, Butcher C, Pathak N, Worswick MJ (2017) Failure parameter identification and validation for a dual-phase 780 steel sheet. Int J Solids Struct 124:89–107. https://doi.org/10.1016/j.ijsolstr.2017.06.018

Bai Y, Wierzbicki T (2008) A new model of metal plasticity and fracture with pressure and Lode dependence. Int J Plast 24(6):1071–1096. https://doi.org/10.1016/j.ijplas.2007.09.004

Barsoum I, Faleskog J (2007) Rupture mechanisms in combined tension and shear-Experiments. Int J Solids Struct 44(6):1768–1786. https://doi.org/10.1016/j.ijsolstr.2006.09.031

Bažant ZP, Vorel J (2014) Energy-Conservation Error Due to Use of Green-Naghdi Objective Stress Rate in Commercial Finite-Element Codes and Its Compensation. J Appl Mech 81(2):021008. https://doi.org/10.1115/1.4024411

Brünig M, Gerke S, Schmidt M (2016) Biaxial experiments and phenomenological modeling of stress-state-dependent ductile damage and fracture. Int J Fract 200(1–2):63–76. https://doi.org/10.1007/s10704-016-0080-3

Butcher C, Abedini A (2017) Shear confusion: Identification of the appropriate equivalent strain in simple shear using the logarithmic strain measure. Int J Mech Sci 134:273–283. https://doi.org/10.1016/j.ijmecsci.2017.10.005

Butcher C, Abedini A (2019) On Phenomenological Failure Loci of Metals under Constant Stress States of Combined Tension and Shear: Issues of Coaxiality and Non-Uniqueness. Metals 9(10):1052. https://doi.org/10.3390/met9101052

Cao TS, Gachet JM, Montmitonnet P, Bouchard PO (2014) A Lode-dependent enhanced Lemaitre model for ductile fracture prediction at low stress triaxiality. Eng Fract Mech 124–125:80–96. https://doi.org/10.1016/j.engfracmech.2014.03.021

Elliott D (1972) Deformation Paths in Structural Geology. Geol Soc Am Bull 83(9):2621. https://doi.org/10.1130/0016-7606(1972)83[2621:DPISG]2.0.CO;2

Ganjiani M, Homayounfard M (2021) Development of a ductile failure model sensitive to stress triaxiality and Lode angle. Int J Solids Struct 225:111066. https://doi.org/10.1016/j.ijsolstr.2021.111066

Grolleau V, Roth CC, Mohr D (2022) Design of in-plane torsion experiment to characterize anisotropic plasticity and fracture under simple shear. Int J Solids Struct 236–237:111341. https://doi.org/10.1016/j.ijsolstr.2021.111341

Habibi N, Zhou M, Lian J, Könemann M, Münstermann S (2023) Numerical investigation into effects of fracture behavior on edge cracking sensitivity. J Mater Process Technol 316:117965. https://doi.org/10.1016/j.jmatprotec.2023.117965

Hancock JW, Mackenzie AC (1976) On the mechanisms of ductile failure in high-strength steels subjected to multi-axial stress-states. J Mech Phys Solids 24(2–3):147–160. https://doi.org/10.1016/0022-5096(76)90024-7

Hossack JR (1968) Pebble deformation and thrusting in the Bygdin area (Southern Norway). Tectonophysics 5(4):315–339. https://doi.org/10.1016/0040-1951(68)90035-8

Hsu TC (1966) The characteristics of coaxial and non-coaxial strain paths. Journal of Strain Analysis. 1(3):216–222. https://doi.org/10.1243/03093247V013216

Johnson GR, Cook WH (1985) Fracture characteristics of three metals subjected to various strains, strain rates, temperatures and pressures. Eng Fract Mech 21(1):31–48. https://doi.org/10.1016/0013-7944(85)90052-9

Lian J, Sharaf M, Archie F, Münstermann S (2013) A hybrid approach for modelling of plasticity and failure behaviour of advanced high-strength steel sheets. Int J Damage Mech 22(2):188–218. https://doi.org/10.1177/1056789512439319

Liu X, Yan S, Rasmussen KJR, Deierlein GG (2022) Experimental investigation of the effect of Lode angle on fracture initiation of steels. Eng Fract Mech 271:108637. https://doi.org/10.1016/j.engfracmech.2022.108637

Lode W (1926) Versuche über den Einfluß der mittleren Hauptspannung auf das Fließen der Metalle Eisen. Kupfer und Nickel Zeitschrift für Physik 36(11–12):913–939. https://doi.org/10.1007/BF01400222

Lou Y, Huh H, Lim S, Pack K (2012) New ductile fracture criterion for prediction of fracture forming limit diagrams of sheet metals. Int J Solids Struct 49(25):3605–3615. https://doi.org/10.1016/j.ijsolstr.2012.02.016

Lou Y, Yoon JW, Huh H (2014) Modeling of shear ductile fracture considering a changeable cut-off value for stress triaxiality. Int J Plast 54:56–80. https://doi.org/10.1016/j.ijplas.2013.08.006

Means WD (1982) An unfamiliar Mohr circle construction for finite strain. Tectonophysics 89(4):T1–T6. https://doi.org/10.1016/0040-1951(82)90138-X

Means WD (1983) Application of the Mohr-circle construction to problems of inhomogeneous deformation. J Struct Geol 5(3–4):279–286. https://doi.org/10.1016/0191-8141(83)90016-0

Mohr D, Marcadet SJ (2015) Micromechanically-motivated phenomenological Hosford-Coulomb model for predicting ductile fracture initiation at low stress triaxialities. Int J Solids Struct 67–68:40–55. https://doi.org/10.1016/j.ijsolstr.2015.02.024

Passchier CW (1988) The use of Mohr circles to describe non-coaxial progressive deformation. Tectonophysics 149(3–4):323–338. https://doi.org/10.1016/0040-1951(88)90181-3

Ramberg H (1975) Particle paths, displacement and progressive strain applicable to rocks. Tectonophysics 28(1–2):1–37. https://doi.org/10.1016/0040-1951(75)90058-X

Ramsay JG, Huber MI. Strain analysis. 7th ed. No. Vol. 1 in The techniques of modern structural geology. London: Academic Press; 2003

Roth CC, Mohr D (2016) Ductile fracture experiments with locally proportional loading histories. Int J Plast 79:328–354. https://doi.org/10.1016/j.ijplas.2015.08.004

Schuster L, Olfert V, Sherepenko O, Fehrenbach C, Song S, Hein D et al (2024) Influences of Weld Nugget Shape and Material Gradient on the Shear Strength of Resistance Spot-Welded Joints. steel research international 95(4):2300530. https://doi.org/10.1002/srin.202300530

Traphöner H, Heibel S, Clausmeyer T, Tekkaya AE (2018) Influence of manufacturing processes on material characterization with the grooved in-plane torsion test. Int J Mech Sci 146–147:544–555. https://doi.org/10.1016/j.ijmecsci.2017.12.052

Traphöner H, Clausmeyer T, Tekkaya AE (2021) Methods for measuring large shear strains in in-plane torsion tests. J Mater Process Technol 287:116516. https://doi.org/10.1016/j.jmatprotec.2019.116516

Vigneshwaran R, Benzerga AA (2023) An analysis of failure in shear versus tension. Eur J Mech A Solids 199:105074. https://doi.org/10.1016/j.euromechsol.2023.105074

Wierzbicki T, Xue L (2005) On the effect of the third invariant of the stress deviator on ductile fracture. Technical report, Impact and Crashworthiness Laboratory, Massachusetts Institute of Technology, Cambridge, MA

Yin Q, Soyarslan C, Isik K, Tekkaya AE (2015) A grooved in-plane torsion test for the investigation of shear fracture in sheet materials. Int J Solids Struct 66:121–132. https://doi.org/10.1016/j.ijsolstr.2015.03.032